Supporting information for

Mixed Mixed Rayleigh-Stoneley modes: Analysis of seismic waveguide coupling and sensitivity to lower-mantle structures

Harry Matchette-Downes[*,1], Jia Shi[2,a], Jingchen Ye[3,4,b], Jiayuan Han[2], Robert D. van der Hilst[1], and Maarten V. de Hoop[2,3]

[*]Corresponding author: hrmd@mit.edu

[1]Department of Earth, Atmospheric and Planetary Sciences, Massachusetts Institute of Technology, 77 Massachusetts Avenue, MA 02139, U.S.A.

[2]Department of Earth, Environmental and Planetary Sciences, Rice University, 6100 Main Street, TX 77005, U.S.A.

[3]Department of Computational and Applied Mathematics, Rice University, 6100 Main Street, TX 77005, U.S.A.

[4]Applied Physics Program, Rice University, 6100 Main Street, TX 77005, U.S.A.

[a]Now at: Shell International Exploration and Production Inc.

[b]Now at: Google LLC.

Contents of this file

- Supplement S1: Group velocity.

- Supplement S2: Projection into unperturbed basis.

- Supplement S3: Effects of rotation.

- Supplement S4: Traveling-wave behavior.

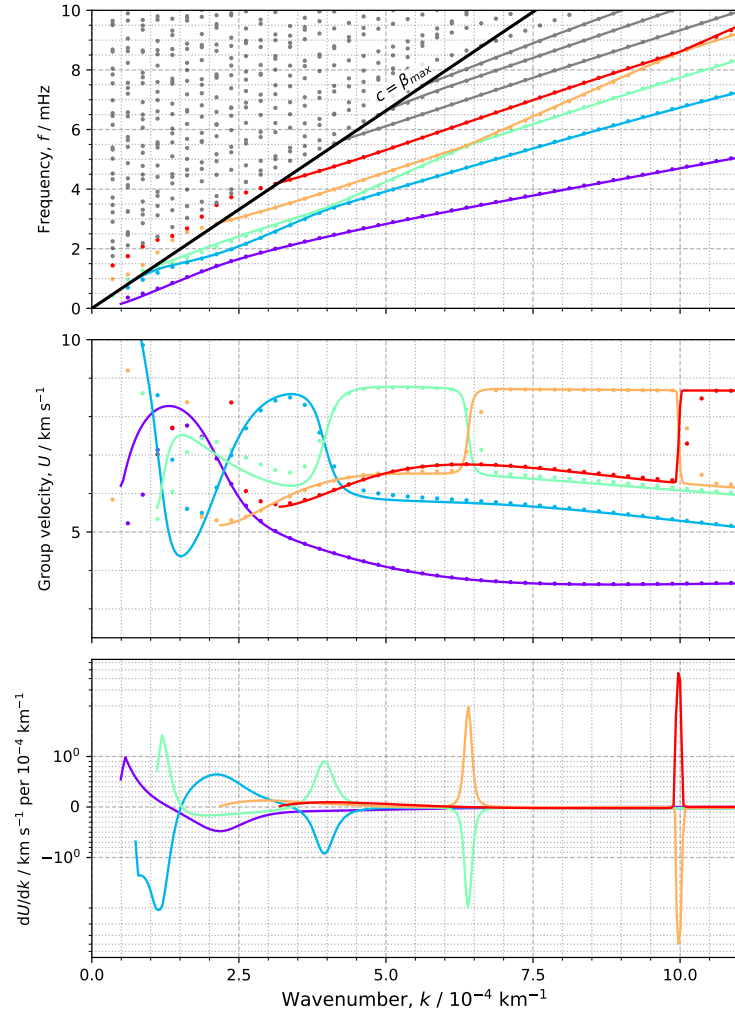- Supplement S5: Mode gallery.

S1 Group velocity

Figure S1: a) Dispersion diagram for modes, shown as points, and the half-space approximation, shown as solid lines. b) Group velocity, calculated from the dispersion diagram, for the first five branches. c) The (continuous) first derivative of the group velocity, illustrating that the group velocity is a smooth function of wavenumber. Note the change from a linear y-axis (between -1 and 1) to a logarithmic one.

S2   Projection of perturbed modes into basis of unperturbed modes

The modes of the spherically-symmetric reference model form a complete basis within the sphere. The perturbed modes can be projected into this basis, as shown here (Supp. Fig. S2) for the lowest-frequency mode of the $_2\mathrm{S}_{16}$ multiplet (see Fig. 4d,f in the main text). The basis functions are normalized using the *Mineos* normalization.

The unperturbed mode basis is used in the perturbation-theory approach to calculate the modes and frequencies of the perturbed model. A common assumption in this approach is the 'isolated multiplet' approximation, where the modes of a perturbed multiplet are calculated using only the modes of the same multiplet, before perturbation, as the basis. The coefficients in Supp. Fig. S2 are mostly close to zero, except for the $_2\mathrm{S}_{16}^m$ coefficients, indicating that the isolated multiplet approximation is a good approximation. However, we can also see weak coupling with $_2\mathrm{S}_{15}$, $_2\mathrm{S}_{17}$, $_1\mathrm{S}_{15}$, $_1\mathrm{S}_{16}$, $_1\mathrm{S}_{17}$, $_6\mathrm{S}_6$ and $_3\mathrm{T}_5$.

The power spectrum of the LLSVP anomaly used in our calculation is shown in Supp. Fig. S3. It is dominated by the $\ell = 1$ band.
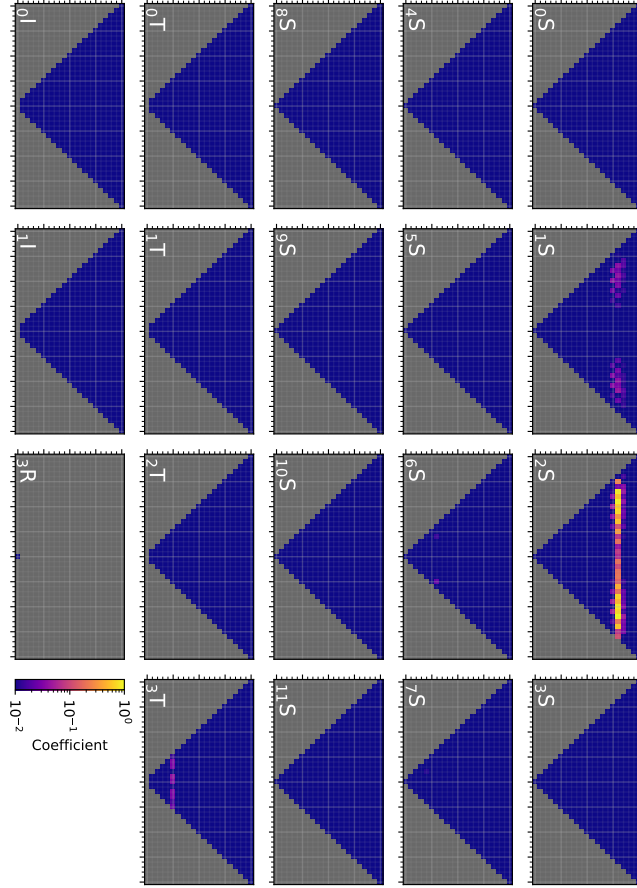
Figure S2: Projection of one of the perturbed modes from the $_2S_{16}$ multiplet into the unperturbed-mode basis. Each panel shows the coefficients $C_{l,m}$ for a given mode branch $_nX$. Only branches with modes within $0.5\,\mathrm{mHz}$ of the the target mode are shown. For each panel, the x-axis corresponds to the angular degree m and the y-axis corresponds to angular order ℓ.
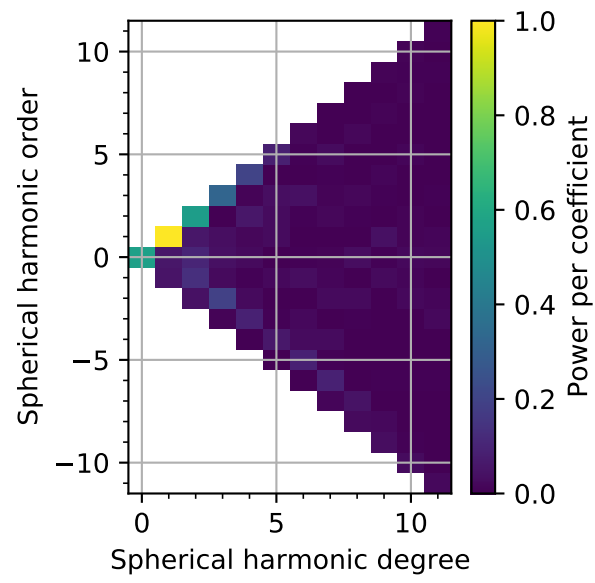
Figure S3: The spherical harmonic power spectrum of the LLSVP anomaly (shown in outline in Fig. 4b,c,d). The power is normalized to the largest coefficient.

S3   Effect of Earth's rotation on the mixed modes

We can make the 3-D mode calculations from the main text (section 3.3) more realistic by including the effects of Earth's rotation: oblateness, centripetal potential, and Coriolis force. Our approach is described in Shi et al. (in review). We assume a rotation period of 23.9345 hours, and calculate the ellipticity as a function of radius using Radau's approximation to Clairault's equation (Dahlen and Tromp, 1998, equation 14.20). Once rotation is including, the eigenfunction vector fields become complex, representing eastward- or westward-propagating waves. The frequencies and spatial displacement patterns are also altered, as we discuss below.

We first note that rotation increases the 'splitting' of each multiplet (which we define as difference between the highest and lowest singlets within a given multiplet). This can be seen by comparing the splitting in the rotating case (Supp. Fig. S4) with the non-rotating case (Fig. 1c); note the change in marker scaling. Although all modes have greater splitting, the splitting of the mixed modes is still markedly stronger due to their sensitivity to the LLSVP anomaly. As an aside, we note that all of the multiplets have a positive shift in their center frequency (the mean of the singlet frequencies).
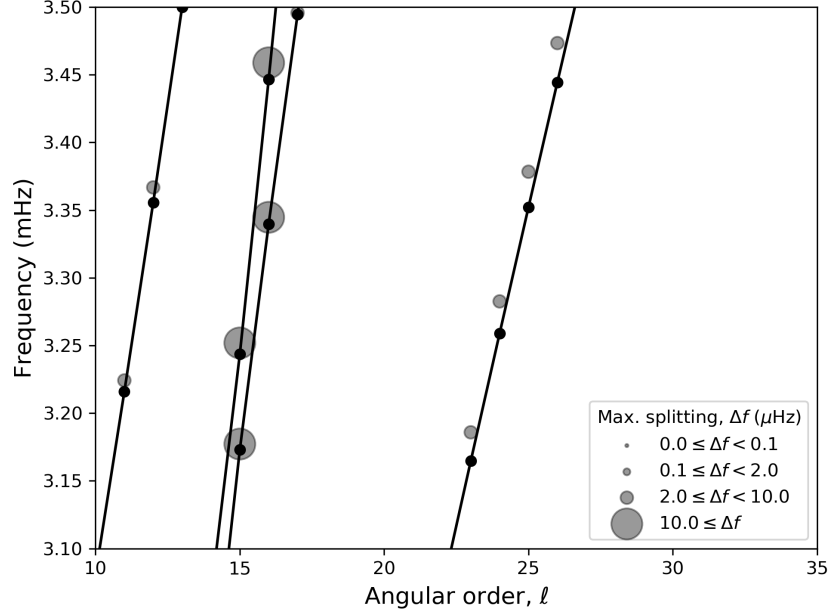
Figure S4: Frequency splitting of each degenerate multiplet in a model with rotation and an LLSVP anomaly. The modes of the spherically-symmetrical reference model are shown as solid lines with opaque dots.

This additional splitting can be understood by examining the eigenfunctions, for example for the mode $_1S_{15}$ in Supp. Fig. S5. As we saw in the non-rotating case (Fig. 4), a range of frequencies arises from modes concentrated inside or outside the LLSVP ('LLSVP-dominated'). This range is augmented by a group of modes whose shape is controlled primarily by Earth's oblate shape ('oblateness-dominated'). These modes have wider, more regular frequency separation, with lower-frequency modes being more concentrated at the equator. Note that the number of singlets does not change.
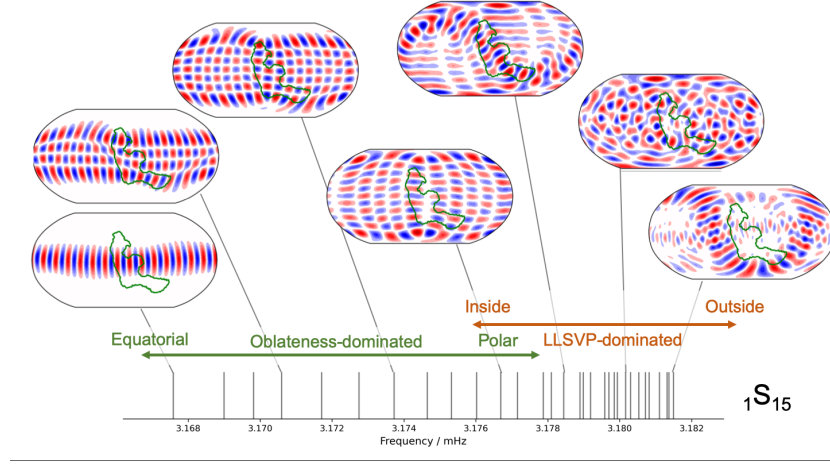
X8

Figure S5: Selected eigenfunctions for multiplet $_1S_{15}$, showing relationship to frequency splitting. Each map shows the real part of the vertical-component displacement field at Earth's surface for a given mode.

This behavior is found in all of the mixed modes and most of the other modes which we calculated (not shown here). A complicating factor is mode coupling, which becomes stronger when rotation is included. We do not discuss mode coupling in detail here, although in future we plan to compare the mode coupling in the direct 3-D approach to the predictions of perturbation theory.

S4 Illustration of traveling-wave behavior

It is well-known that summation of normal modes along a branch yields a traveling wave. We investigated whether summation of the modes of the second quasi-intersection produces any unusual traveling-wave behavior. The modes used in the summation are shown in Supp. Fig. S6. Each mode marker is scaled according to the globally-averaged RMS excitation of that mode, given our choice of source, which was the point CMT approximation of the 2011 Tohoku earthquake. Note that these calculations were carried out in $Mineos$ and include the effect of attenuation, unlike other mode calculations in this paper.

We restricted the summation to modes from the two intersecting branches ($n = 2$ and $n = 3$) within a narrow frequency band indicated by the outer pair of gray horizontal lines. A cosine frequency taper was applied to this band, so that modes outside the inner pair of gray horizontal lines had reduced amplitude. It can be seen that the Stoneley branch has low excitation amplitudes, typically around 100 times weaker than the Rayleigh branch.

The contributions of the two branches can be visualized in Supp. Fig. S7. From the left column, we see that the Rayleigh branch resembles a traveling wave in the middle and upper mantle, but in the lower mantle it resembles a standing wave, due to contributions from just a small number of mixed modes at these depths. The middle column shows that the Stoneley branch resembles a standing wave throughout the planet, because only a few modes are excited. The net effect, shown in the right column, appears to have a traveling wave in the upper mantle and on the CMB.

We can understand the results of the full summation by plotting the velocity field as a seismic section with increasing distance from the source (Supp. Fig. S8). The plot also shows the group velocities of the modes (calculated using $Mineos$) for a selection of modes. The wavefield at the surface is a traveling wave whose group velocity is well described by the 'normal' Rayleigh modes before and after the quasi-intersection region (e.g. modes $_3S_{22}$ and $_2S_{28}$). In other words, the surface wavefield is dominated by the second Rayleigh overtone.

X10

By contrast, if we plot the wavefield just above the core-mantle boundary (Supp. Fig. S9), a different traveling wave arises. This wavepacket is more dispersive, with group velocities ranging between the Rayleigh and Stoneley group velocities found further from the intersection. Note that the amplitude of this wave is around 10 times smaller than the surface wave.

We interpret this CMB wave in the following way: near the quasi-intersection, the Rayleigh modes have a small Stoneley component at the CMB, and the Stoneley modes have a small Rayleigh component at the surface. When carrying out the normal-mode summation near the quasi-intersection, if all of these modes are included, the excitation amplitudes are large enough over a sufficiently wide bandwidth to produce a traveling wave on the CMB. The wavepacket is broad due to the wide range of group velocities of the contributing modes. We call this a 'mixed Stoneley-Rayleigh wave'

Unfortunately, if a corresponding 'mixed Rayleigh-Stoneley wave' exists and propagates along the free surface, its amplitude must be very small as it is not visible in Supp. Fig. S8. Therefore, although it is interesting to know about the CMB wave, it is not of practical use.
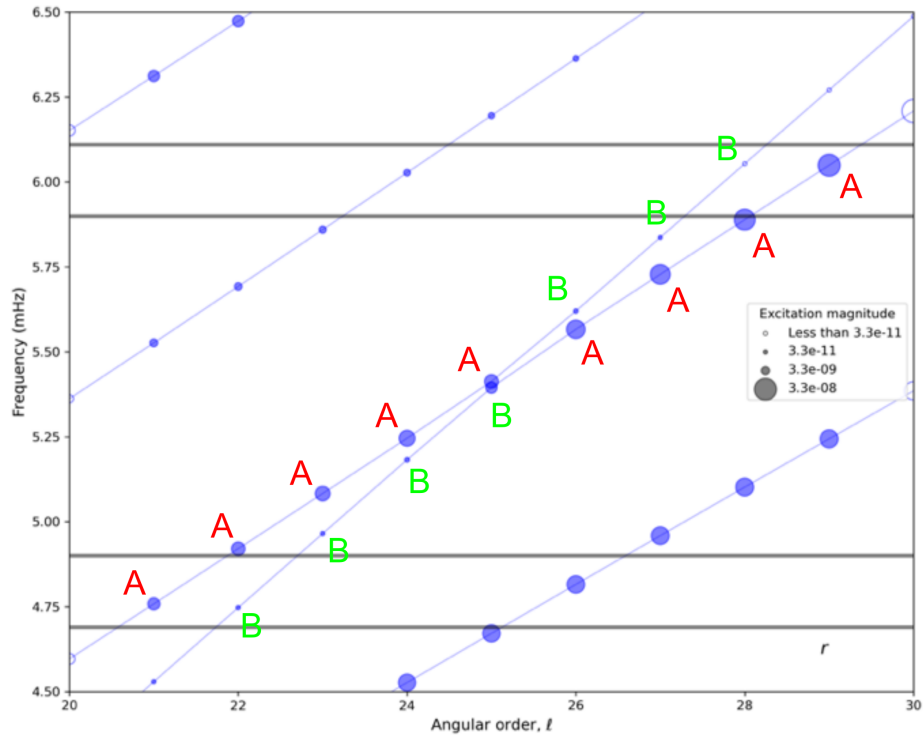
Figure S6: Mode diagram showing detail of the second quasi-intersection. Marker symbols are scaled by the excitation of each mode (in S.I. units). Second-overtone Rayleigh modes are labeled 'A', and Stoneley modes are labeled 'B' (although this distinction is arbitrary in the case of the mixed modes).
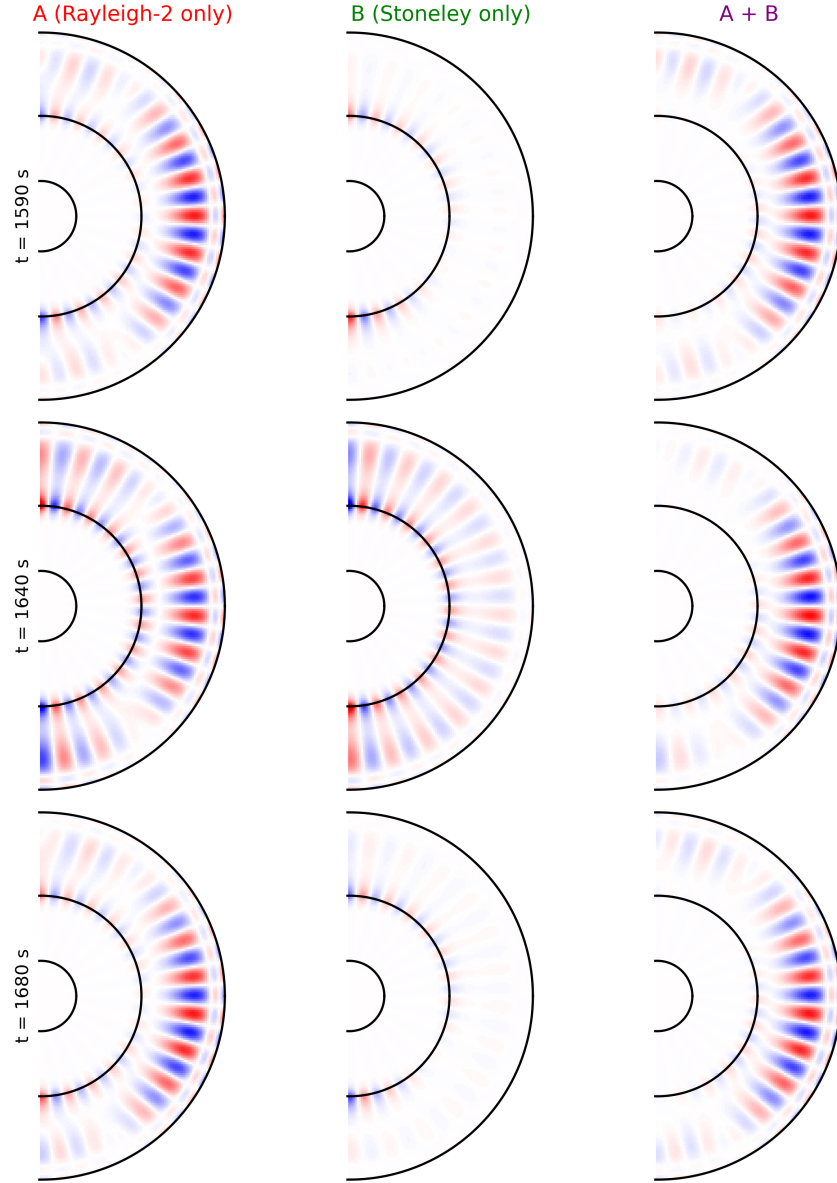
Figure S7: Plots of the vertical velocity field at various times (indicated on the left-hand side) after the earthquake, decomposed into contributions from different mode branches (indicated at the top). The color scale is the same for each panel. The source location is at the top of each panel.
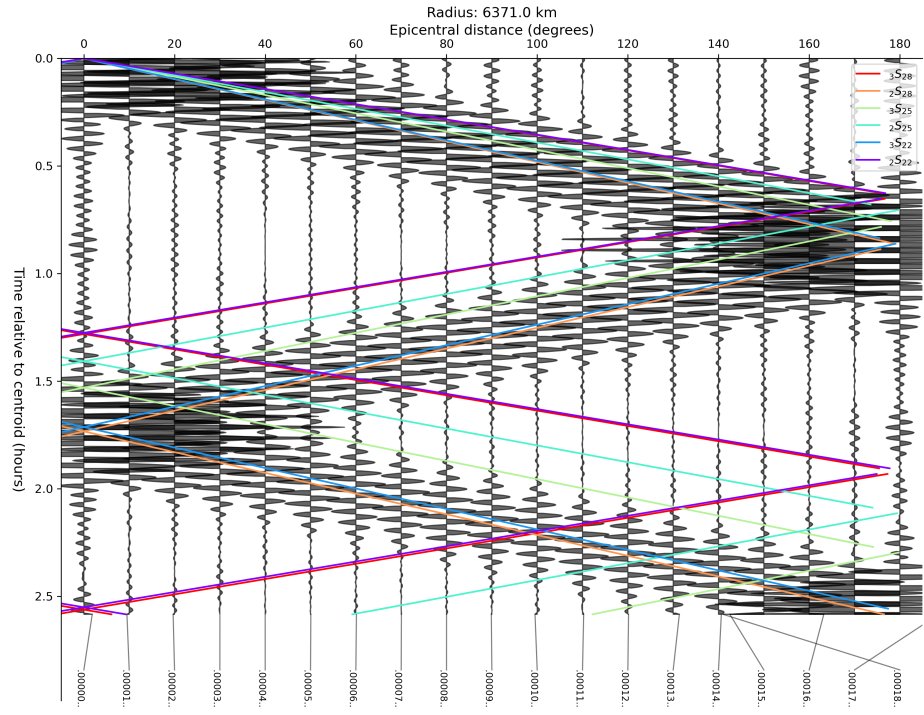
Figure S8: Seismic section observed at the surface. Each trace shows the particle velocity at the specified epicentral distance. Traces are normalized by a common value so that relative amplitudes are preserved. Mode group velocities are indicated by colored lines as shown in the legend.
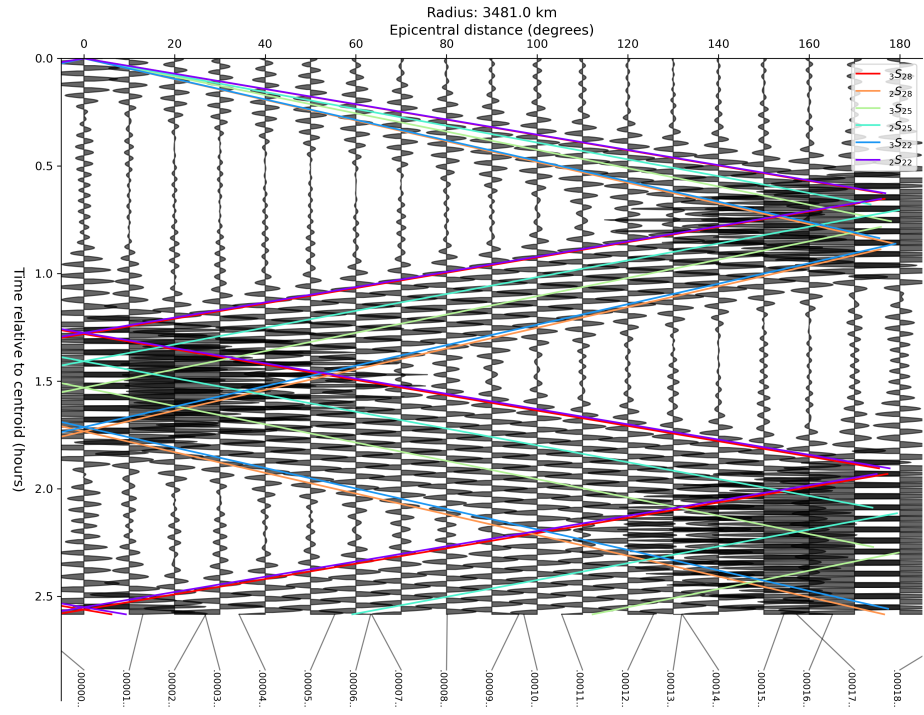
Figure S9: The same as Supp. Fig. S8, except the particle velocity is plotted at the CMB instead of the surface.

S5 Gallery of modes near quasi-intersections

Here we show the eigenfunctions for modes in the vicinity of the first, second and third quasi-intersections, calculated using the *Mineos* code. In contrast with the main text, we include the effects of attenuation and the perturbation to the gravitational potential, to make these calculations as realistic as possible. Nonetheless, given that mode mixing is sensitive to small shifts in mode frequencies, this gallery should not be used to pin-point mode-mixing frequencies on the real Earth, because we have neglected the effects of anisotropy, rotation, and three-dimensional structures, including ellipticity and the crust and ocean.
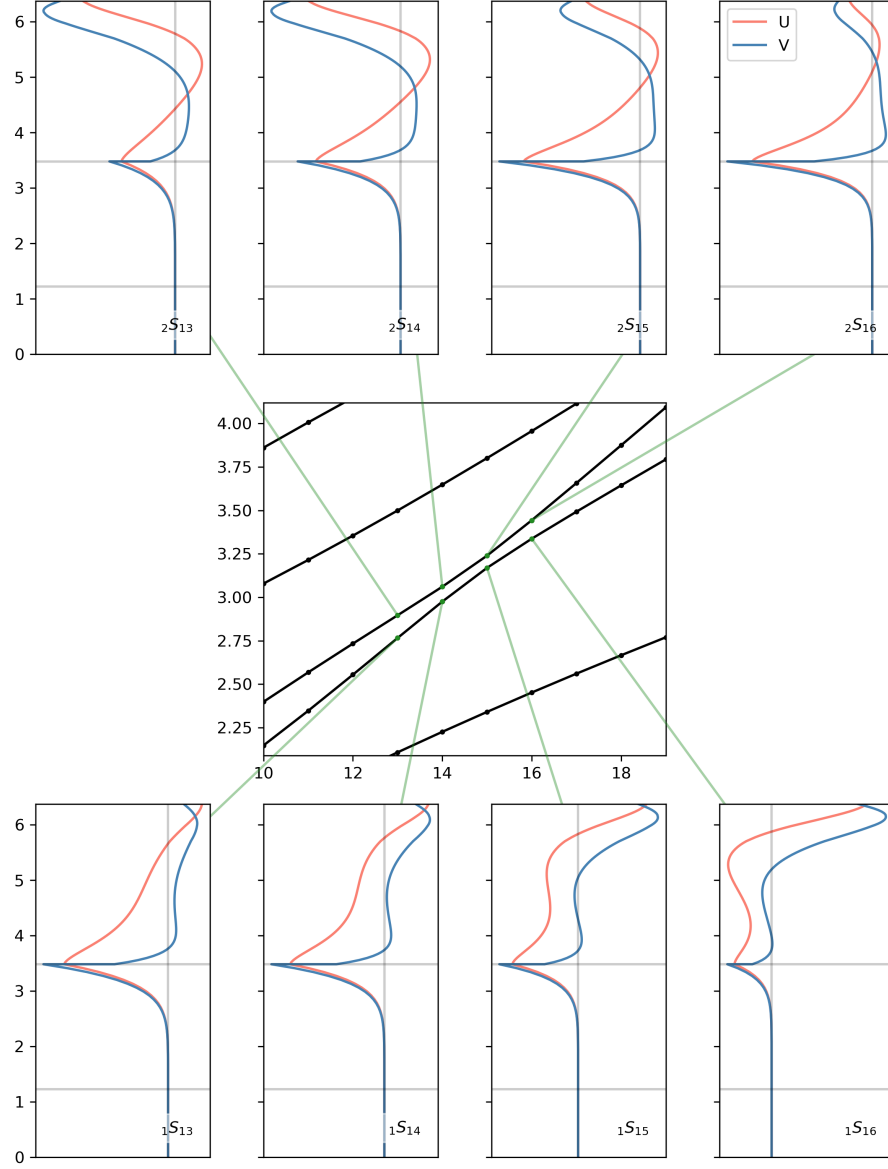
Figure S10: Summary of eigenfunctions of modes near the first quasi-intersection. The central panel shows the location of the modes on the dispersion diagram (ℓ versus frequency in mHz). For each mode, the radial and consoidal components are shown, including the factor of k omitted in some conventions. The y-axis shows radial coordinate in units of 10^3 km and horizontal lines indicate the CMB and ICB discontinuities.
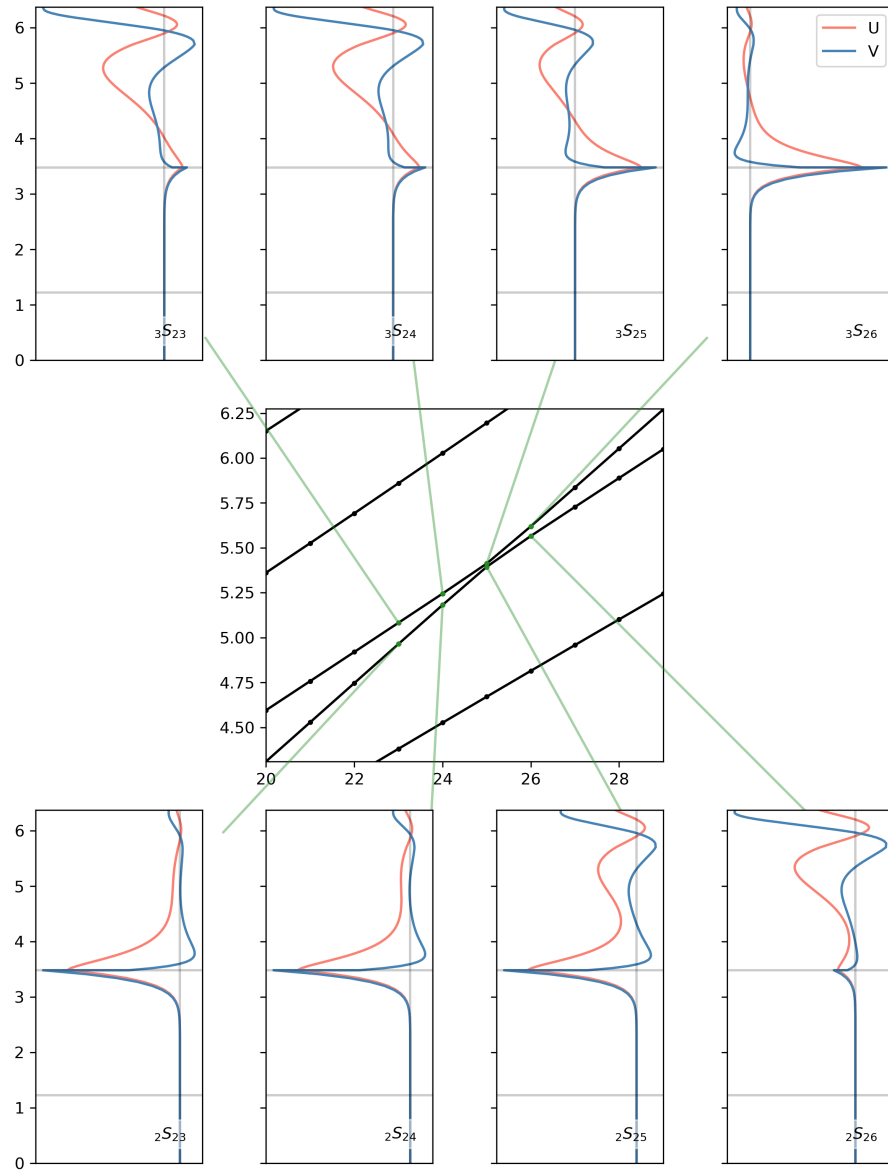
X17

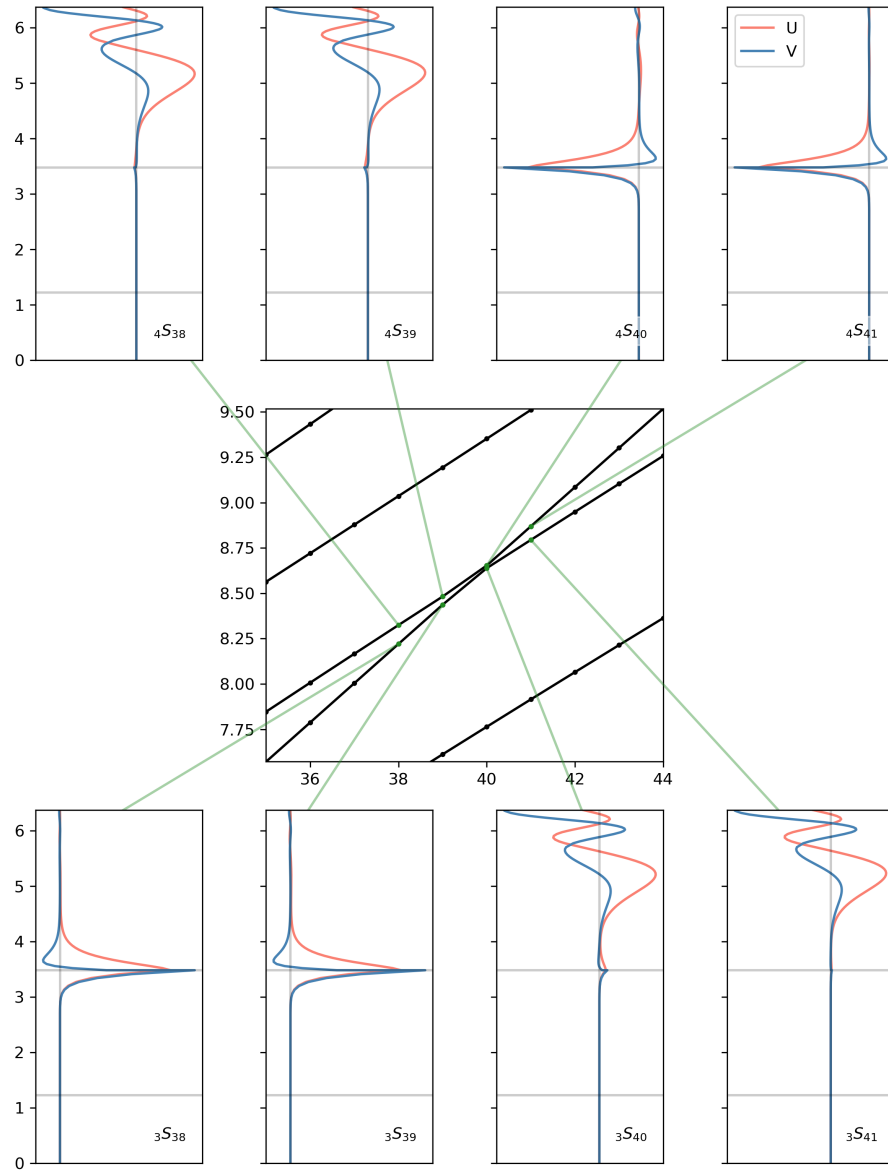Figure S11: Same as Supp. Fig. S10, but for the second quasi-intersection.

Figure S12: Same as Supp. Fig. S10, but for the third quasi-intersection.